ACS Photonics

pubs.acs.org/journal/apchd5

Article

Omnidirectional Gradient Force Optical Trapping in Dielectric Nanocavities by Inverse Design

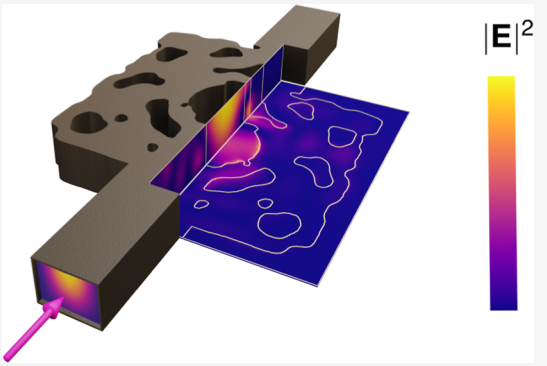
Beñat Martinez de Aguirre Jokisch,* Benjamin Falkenberg Gøtzsche,* Philip Trøst Kristensen,* Martijn Wubs,* Ole Sigmund,* and Rasmus Ellebæk Christiansen*

Cite This: *ACS Photonics* 2024, 11, 5118−5127

Read Online

ACCESS | Metrics & More | Article Recommendations | Supporting Information

ABSTRACT: Optical trapping enables precise control of individual particles of different sizes such as atoms, molecules, or nanospheres. Optical tweezers provide free-space omnidirectional optical trapping of objects in laboratories around the world. As an alternative to standard macroscopic setups based on lenses, which are inherently bound by the diffraction limit, plasmonic and photonic nanostructures promise trapping by near-field optical effects on the extreme nanoscale. However, the practical design of lossless waveguide-coupled nanostructures capable of trapping subwavelength-sized particles in all spatial directions has until now proven insurmountable. In this work, we demonstrate an omnidirectional optical trap realized by inverse-designing fabrication-ready integrated dielectric nanocavities. The subwavelength optical trap is designed to rely solely on the gradient force and is thus particle-size-agnostic. In particular, we show how a trapped particle with a radius of 15 nm experiences a force strong enough to overcome room-temperature thermal fluctuations. Furthermore, through the robust inverse-design framework, we tailor manufacturable devices operating at short-wave-infrared and near-infrared wavelengths. Our results open a new regime of levitated optical trapping by achieving a deep trapping potential capable of trapping single subwavelength particles in all directions using optical gradient forces. We anticipate potentially groundbreaking applications of the optimized optical trapping system for biomolecular analysis in aqueous environments, levitated cavity optomechanics, and cold atom physics, constituting an important step toward realizing integrated bionanophotonics and mesoscopic quantum mechanical experiments.



KEYWORDS: *inverse design, topology optimization, optical trapping, dielectrics, optomechanics, biophotonics*

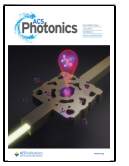
Downloaded via DTIC NATL TECH INFORMATION CTR on July 2, 2026 at 15:41:34 (UTC).
See https://pubs.acs.org/sharingguidelines for options on how to legitimately share published articles.

INTRODUCTION

Optical tweezers are versatile tools for interdisciplinary research due to their precise control and manipulation of micron-sized objects.[1] With applications ranging from studies in microbiology[2,3] to fundamental physics research,[4−6] the optical tweezer is a decorated research tool. Undoubtedly, the success of the optical tweezer is owed to its ability to omnidirectionally trap objects by use of a single laser; however, since it is based on free-space optics, it is inherently bound by the diffraction limit. This limit can result in prohibitive power requirements to trap nanometer-scaled particles. As shown in ref 7, a micrometer-sized polystyrene sphere can be stably trapped—stable against thermal diffusion of the particle—by an optical tweezer with a fraction of a milliwatt, while a 10 nm sphere requires 1.5 W. To overcome this power limitation, nanostructured metallic devices have been employed,[8−10] which can achieve stable trapping of nanometer-scaled particles at much lower powers, utilizing the strongly localized optical forces of plasmonic resonances. Such plasmonic devices have successfully been applied to the optical trapping of single proteins[10] and single particle Raman spectroscopy,[9] among others. However, inherent losses in metals lead to heating and potential stability concerns of the electromagnetic resonator or adverse effects on the trapped objects.[11−14] To solve these issues, near-lossless nanostructured dielectric optical traps have been proposed.[11,12,15,16] Experimental realizations of dielectric traps include the trapping of single quantum dots[11] and the trapping of particles utilizing Fano resonances,[15] to name a few.

Recent developments in the design and fabrication of dielectric bowtie-based nanocavities suggest access to hitherto unexplored field strength in dielectrics with deeply subwavelength light confinement.[17−19] Bowtie nanocavities have previously been used as efficient optical traps[20−22] by utilizing the strong field enhancements at the material interfaces.[23−25] However, this field enhancement inevitably makes the particle

Received: June 11, 2024
Revised: September 13, 2024
Accepted: September 16, 2024
Published: September 24, 2024



© 2024 The Authors. Published by American Chemical Society

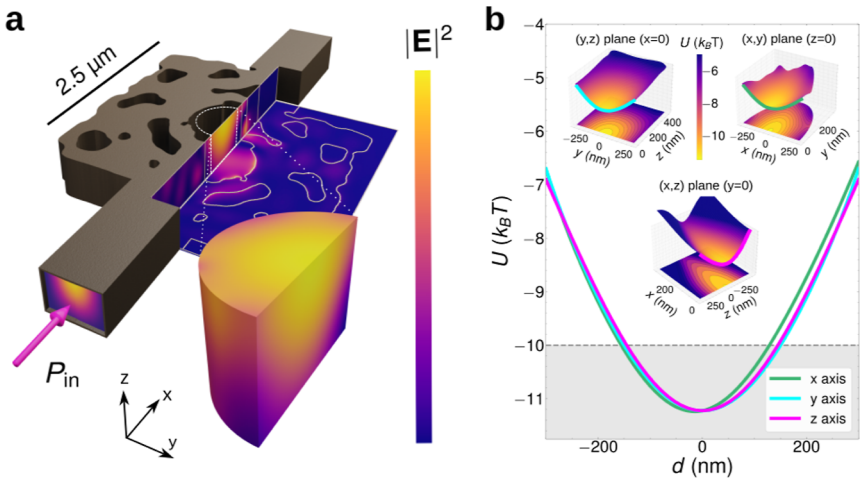


Figure 1. Optical response and trapping potential for the inverse-designed structure. (a) Rendering of the lower half of the optimized structure, with the electric field intensity $|\mathbf{E}|^2$ response at $\lambda = 1.55\ \mu$m, with a zoom-in in the optimization region (Ω), when excited with the fundamental mode of the waveguide at an input power $P_{in} = 60$ mW. (b) Trapping potential in the optimization region for the axial line and plane cuts as a function of the distance from the center (d). The stable trapping regime below $U = -10\ k_BT$ is shown in gray.

stick to the resonator walls,[20,22] impeding omnidirectional trapping with gradient forces. For mesoscopic quantum mechanical experiments, any contact with the resonator material is detrimental to the coherence of the prepared state,[4] and in biomolecular analysis, it may lead to undesired charge reconfiguration.[26]

In this work, we directly address the issue of omnidirectional trapping in nanostructures by inversely designing dielectric nanocavities that trap particles with sizes significantly below the diffraction limit. A recent study[16] addresses the issue of omnidirectionality for a limited range of particle sizes by utilizing gradient forces and self-induced back-action (SIBA) effects.[27] Here, by only relying on gradient forces, we deterministically tailor the device geometry of a nanostructure to feature a particle-size-independent omnidirectional trapping potential. The inverse-design process relies on topology optimization (TO), a design optimization method widely used in the design of optical applications like waveguides,[28,29] cavities,[18,30,31] demultiplexers,[32] microresonators,[33] and more. Experimental evidence[18] shows that topology-optimized structures can directly incorporate manufacturing constraints,[34,35] ensuring precise fabrication of optimized device blueprints. In a recent work, a plasmonic optical trap was designed using TO by maximizing the electric field strength at the center of a cavity,[60] yielding the well-known bowtie-like structure, that can trap particles at the material interfaces. In this work, we employ a novel TO scheme based on fitting the electromagnetic field profile to a desired Gaussian shape, enabling omnidirectional trapping within a specified volume. This scheme represents a versatile framework that can design optical traps for arbitrary material platforms, wavelengths, particle choices, and homogeneous background media. Using this framework, we design two different waveguide-coupled and fabrication-ready devices at different wavelengths and homogeneous background materials, which may pave the way for future on-chip levitated optomechanics, on-chip biomolecular analysis,[61] and cold-atom-based quantum many-body systems.[36]

METHODS

Inverse-Designing Omnidirectional Trapping. To trap particles with a radius $R \ll \lambda$, where λ is the wavelength of light, we may apply the dipole approximation.[37] To show that our results apply to a wide range of lossless particles, we consider a nonresonant spherical particle with refractive index $n = 2$ and radius $R = 15$ nm, representative for both proteins ($n \simeq 1.6$, $R \in [1-100\ \text{nm}]$)[12,38] and semiconductor quantum dots ($n \simeq 2.4$, $R \in [2-50\ \text{nm}]$).[12,39−41] For our choice of a lossless and nonresonant isotropic particle, scattering forces are negligible, and the force may thus be well-approximated by the gradient force. This conservative force can be described as the gradient of the trapping potential[37]

$$U(\mathbf{r}) = -\frac{\alpha_R}{4}[\mathbf{E}^*(\mathbf{r})\cdot\mathbf{E}(\mathbf{r})] \tag{1}$$

where $\mathbf{E}$ is the electric field phasor, $\mathbf{E}^*$ denotes its complex conjugate, and α_R is the real part of the spherical particle's polarizability, as given by the Clausius−Mossotti relation.[37] Therefore, for a given particle in the nanostructure, the trapping potential is directly described by calculating the electric field distribution of the empty cavity. The dipole approximation may, however, break down for particles that are larger, exhibit loss, are resonant, or possess a higher refractive index, where additional effects like SIBA or scattering forces (e.g., radiation pressure or spin-curl forces)[37,42] may need to be accounted for. In postanalysis, we verify that our devices are unaffected by any of these effects.

To model optical trapping in the dipole approximation, we calculate the electric field of the empty cavity by solving Maxwell's equations in the frequency domain, assuming time-harmonic behavior.[37] The model is discretized and solved using the finite-element method with first-order Nedelec elements.[43] The trapping device consists of two silicon waveguides connected to a central design domain, in which TO is applied; see Figure 1a. The central region contains a cylindrical air exclusion region with a radius of $R_{exc} = 300$ nm and a thickness of 800 nm, in which the stable trap is located. One of the waveguides is excited with the fundamental mode at an input power of $P_{in} = 60$ mW and a free-space wavelength of λ. The wavelength is a freely selectable design parameter, determined by the desired application of the trap. Here, as a demonstration, we inverse-design a device in the short-wave-infrared regime ($\lambda = 1.55\ \mu$m), and in one of the following sections, we inverse-

https://doi.org/10.1021/acsphotonics.4c01060
ACS Photonics 2024, 11, 5118−5127

design an optical trap in the near-infrared regime ($\lambda = 775$ nm). The material distribution in the design domain is optimized to obtain an electric field distribution that results in an omnidirectional trapping potential. Accordingly, we formulate our design problem as a continuous optimization problem where the material distribution is controlled by our design parameters and where we seek to minimize a figure of merit (FOM) that defines the difference of the electric field norm with respect to the reference field $\mathbf{E}_{\mathrm{ref}}$. This expression may be written as

$$\mathrm{FOM} \equiv \Phi = \sqrt{\int_{\Omega} \left[\Theta\left(\frac{\|\mathbf{E}(\mathbf{r})\|}{\|\mathbf{E}(\mathbf{r}_0)\|} - \frac{\|\mathbf{E}_{\mathrm{ref}}(\mathbf{r})\|}{\|\mathbf{E}_{\mathrm{ref}}(\mathbf{r}_0)\|} \right) \right]^2 \mathrm{d}\Omega} \tag{2}$$

where $\mathbf{r}_0$ is the center point in the design domain, $\Theta(x)$ is a smoothed Heaviside threshold function,[44] and Ω is the optimization domain defined by the exclusion region, see Figure 1a. The FOM takes the form of a p norm with $p = 2$, allowing a homogeneous penalization of the differences over optimization domain Ω. To ensure subwavelength omnidirectional trapping, we select the reference field to be a three-dimensional Gaussian potential with standard deviations $\sigma_x = \sigma_y = 300$ nm and $\sigma_z = 400$ nm to ensure that it features a stable trapping minimum in all spatial directions. In this expression, the Heaviside projection $\Theta(x)$ ensures that the FOM promotes only electric field distributions as steep as or steeper than the target field. If $\Theta(x)$ had not been applied, then the difference to the target distribution would be minimized, not allowing for steeper trapping potentials and thus overconstraining the optimization problem by only fitting the target distribution. The standard deviations are chosen to match the dimensions of the cylindrical exclusion nanocavity with a volume V_{cav} below the diffraction limit: $V_{\mathrm{cav}} = 0.22\ \mu\mathrm{m}^3 < (\lambda/2)^3 = 0.465\ \mu\mathrm{m}^3$. Additionally, we control the minimum depth of the trapping potential by adding a constraint to the optimization problem, which prescribes a minimum electric field norm value at $\mathbf{r}_0$: $\log_{10}(\|\mathbf{E}(\mathbf{r}_0)\|) \geq \gamma$, where γ is a problem-dependent parameter defined in the Supporting Information. By enforcing the constraint, the optimizer avoids local minima where the trapping potential has the correct shape but is not deep enough for stable trapping. To ensure the manufacturability of the device, we add a constraint to connect the design to the two waveguide ends[35] as well as two minimum length scale constraints that act on the solid and void regions, respectively.[34] To minimize the constrained FOM, we apply TO on the design domain, introducing one design variable per finite element in our discretized design domain, which is used to interpolate between air (0) and silicon (1). The design variables are fixed to only vary in the (x, y) plane and are linked in the z direction.[45] We apply a filtering and thresholding procedure to regularize the design.[44] The filtered and thresholded design variables are related to the material's refractive index through a material interpolation scheme.[46] The optimized design is obtained by solving the TO problem from a single uniform initial guess, using the globally convergent method of moving asymptotes as the optimizer.[47] All inverse-design problems are solved using COMSOL Multiphysics[48] executed on the DTU Computing Center HPC cluster.[49] For more information on the forward problem, the inverse-design framework, and the full optimization problem, see the Supporting Information.

RESULTS AND DISCUSSION

Inverse-Designed Nanocavity in the Short-Wave Infrared. The inverse-designed omnidirectional trap and its key characteristics are presented in Figure 1. In Figure 1a, we show the electric field intensity for the optimized structure in the short-wave infrared, which has a well-defined bell-shaped curve in all spatial directions. This is confirmed by observing the different plane and line cuts for the trapping potential in Figure 1b. One can identify a minimum of the potential at the optimization region's center, resulting in an omnidirectional trapping potential. Interestingly, the potential has a similar shape in all directions, meaning that the Heaviside projection $\Theta(x)$ in the FOM allowed the potential to become steeper than the reference Gaussian along the z axis. For the 60 mW of optical input power and the reference particle with $R = 15$ nm and $n = 2$, the trapping minimum is stable against thermal fluctuations at room temperature ($T = 300$ K), which conventionally requires a characteristic trapping depth of $U \simeq -10\ k_{\mathrm{B}}T$,[37] where k_{B} is the Boltzmann constant. Note that as long as the dipole approximation is valid and for high enough input power, the proposed device can stably trap arbitrarily small dielectric spheres in all directions.

From the potential in the dipole approximation, we calculate the axial components of the force experienced by the particle in Figure 2a. Specifically, we show that close to the origin, the force

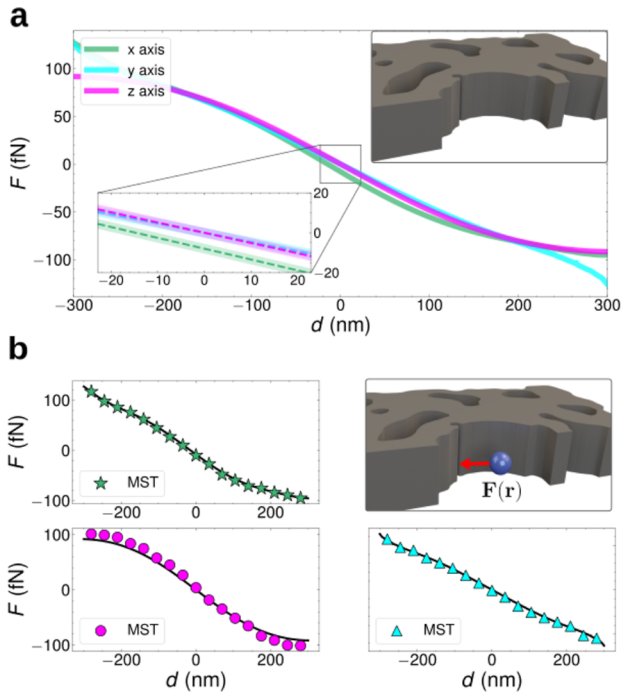


Figure 2. Trapping force calculation and MST validation. (a) Trapping force for the empty cavity in the dipole approximation for the axial components. (b) Force calculations via the MST for different particle positions, compared to the dipole approximation prediction (black line).

becomes linear to a good approximation, and thus, the particle-trap system behaves as a linear spring-mass system. The force in the linear region can then be written as $F_i(r_i) = \kappa_i \cdot r_i$, where $i \in \{x, y, z\}$ is an axis index, κ is a vector with the axial components of the trapping stiffness, and r_i is the position on the axis. Fitting the curves in the central region with a linear function yields trapping stiffnesses of $\kappa_x = 0.53$ fN/nm, $\kappa_y = 0.46$ fN/nm, and $\kappa_z = 0.51$

https://doi.org/10.1021/acsphotonics.4c01060
ACS Photonics 2024, 11, 5118−5127

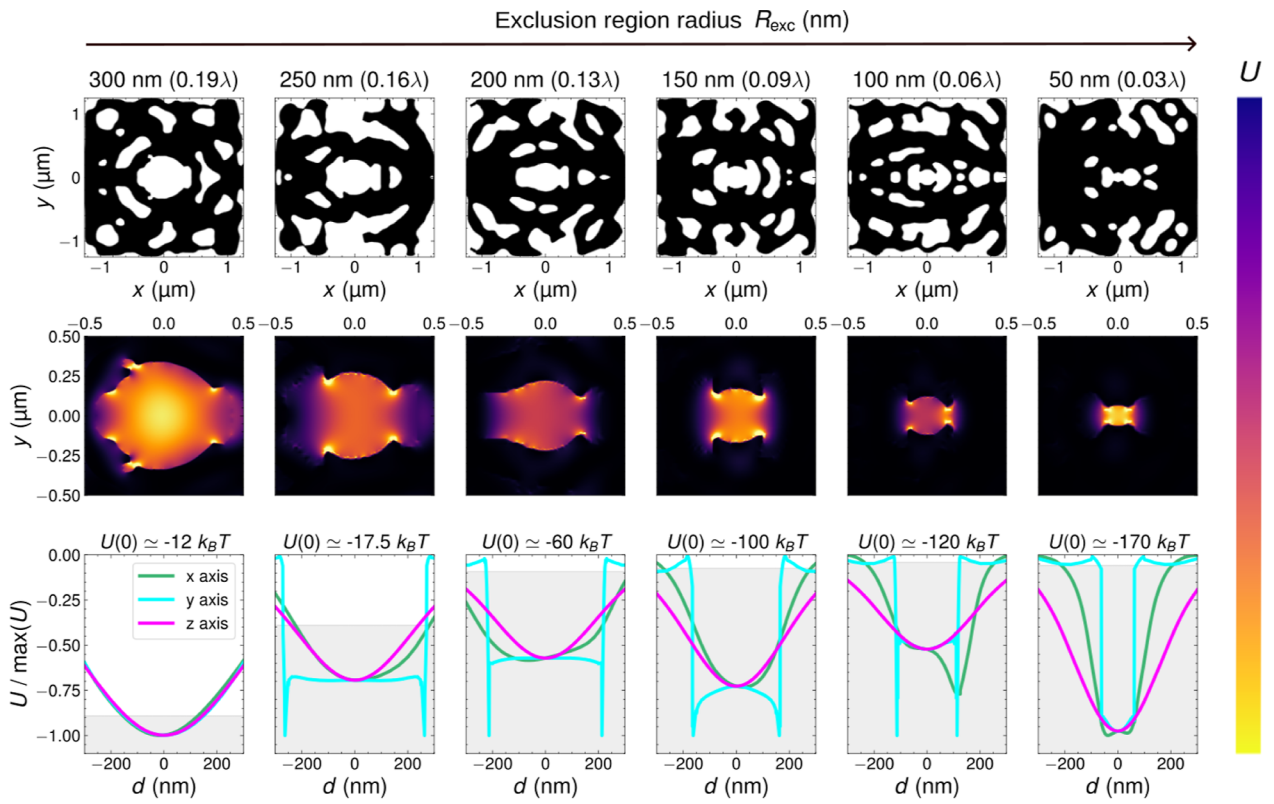


Figure 3. Projection of the nanocavity designs in the (x, y) plane for decreasing radii of the exclusion region (R_{exc}), the spatial distribution of the optical trapping potential U in the (x, y) plane, and the projection of the max-normalized trapping potential on the Cartesian axes. In the designs, black represents silicon and white represents air. The stable trapping regime below $U = -10\ k_BT$ is shown in gray in the trapping potential projection onto the Cartesian axes.

fN/nm. It is possible to compare this device to conventional optical tweezers by comparing their trapping stiffnesses. The transverse trapping stiffness for a free-space optical tweezer is given by ref 4

$$\kappa_{OT} = 4\pi^3 \frac{\alpha_R P_{in}}{c\varepsilon_0} \frac{NA^4}{\lambda^4} \tag{3}$$

where the subscript OT refers to optical tweezers, c is the speed of light, ε_0 is the vacuum permittivity, and NA is the numerical aperture. For a NA = 0.8, as chosen in ref 4, the trapping stiffness is $\kappa_{OT} \simeq 0.03$ fN/nm. In comparison to this reference, our device outperforms conventional optical tweezers by more than an order of magnitude in all three directions.

To validate the dipole approximation, we solve the full Maxwell's equations with the sphere (R = 15 nm and n = 2) present in the optimized geometry and calculate the force using the Maxwell Stress Tensor (MST) formalism.[37] In Figure 2b, we show the axial components of the force experienced by the particle when displaced in increments of 35 nm in the three directions. By comparing the force derived from the MST calculation and the dipole approximation, we confirm that there is excellent agreement between the results and that there are no other dominant effects, such as SIBA,[27,50] or scattering forces.[37,42] By systematically increasing the particle size, it is shown[51] that the dipole approximation holds within a maximum relative error of 15% for particles with sizes up to R = 100 nm and refractive indices up to n = 8, which shows the robustness of the presented methodology.

Tuning the Exclusion Radius: from the Omnidirectional Trapping Regime to the Strong Light Confinement Regime. One of the parameters that requires the most careful tuning in the inverse-design procedure is the radius of the exclusion region (R_{exc}). In principle, to achieve the highest possible trapping stiffness, which is defined as the force exerted over a distance, one would try to make the exclusion region as small as possible. This would allow for stronger light confinement on a subwavelength scale, enhancing the trapping stiffness. However, through systematic optimizations selecting different exclusion radii and accordingly different standard deviations of the target trapping potential (σ_x and σ_y), we find a trade-off between the increased trapping stiffness and the possibility of achieving omnidirectional trapping with gradient forces. This is summarized in Figure 3, where for decreasing exclusion region radii and standard deviations of the target trapping potential, we optimize six nanocavity designs and calculate their trapping potential. The cavities optimized for smaller exclusion region radii can achieve strong field enhancements below the diffraction limit, providing deep trapping potentials. In fact, and based on the bowtie-like cavity design for the smallest exclusion region (R_{exc} = 50 nm), we see that if dielectric material was allowed in the exclusion region, the optimizer would create extreme dielectric confinement bowtie-like cavities, similar to ones in refs 18 and 19. However, similar to bowtie-like cavity designs,[20−22] when checking the trapping potential distribution for exclusion radii below R_{exc} = 200 nm in Figure 3, it is clear that the strong field confinement located at the material interfaces does not allow for an omnidirectional trap in the center of the cavity due to the spatial overlap of the field from the tip-like structures close to the center. This is similar to the double nanohole structure with a deeply subwavelength exclusion

https://doi.org/10.1021/acsphotonics.4c01060
ACS Photonics 2024, 11, 5118−5127

region found by another inverse-design work[60] where the electric field was maximized at the center of the cavity, yielding a bowtie-like nonomnidirectional trapping potential. Interestingly, even for an exclusion radius of R_{exc} = 250 nm, the trapping potential in the y direction starts to lose its concavity, which is further accentuated for smaller radii. In other words, there is a minimum length scale of the exclusion radius close to $R_{exc} \simeq 250$ nm, which sets a geometrical limit on omnidirectional trapping. By observing the projection of the trapping potential onto the Cartesian axes, it seems, however, that one recovers stable trapping when going down to the smallest exclusion radius (R_{exc} = 50 nm), but by looking at the two-dimensional profile of the trapping potential, it is evident that a particle would be trapped at the nanocavity tips, where the field enhancement is strongest. In our work, we choose an exclusion radius R_{exc} = 300 nm since it simultaneously allows for an omnidirectional trapping without compromising the depth of the trapping potential or the trapping stiffness. This parameter choice allows trapping deeply subwavelength particles in a subwavelength exclusion region while overcoming thermal fluctuations.

Vacuum Surface Forces: Casimir–Polder Forces. We have shown that once the particle is at the center of the trap, it will be omnidirectionally trapped. However, loading the particle into the trap may potentially be jeopardized by other physical effects such as the field enhancement observable at the bottom interface of the structure in Figure 1a or the Casimir–Polder (CP) forces near the material interfaces. In section S3.1 of the Supporting Information, we study the optical forces at the surfaces due to strong optical field enhancements, also known as lightning-rod effects,[24,25] and estimate the probability of a particle sticking to the surface due to these forces. In this section, we study CP forces,[52] which are vacuum forces that also exist in the absence of a light source and result in a net attractive force to the surface that scales nonlinearly with the distance between the particle and the surface. To calculate the probability of the particle getting stuck at the interface due to CP forces, we approximate the nanosphere as a polarizable point dipole, close to an infinite dielectric plane, which is a good approximation since the CP forces are known to dominate only at short length scales on the order of 10 nm (see below). Given the high symmetry of this system, the CP energy landscape of this system reduces to a function of the distance d between the center of the particle and the plane. Following the derivation in ref 53, we calculate this function by integration of the Green tensor as formulated in ref 54. We show the CP energy landscape as a normalized trapping potential in Figure 4 at room temperature (where k_BT = 0.025 eV), for a particle with a refractive index n = 2 and a radius of R = 15 nm, close to an infinite silicon interface with a refractive index n = 3.48.

In the simplified model, the trapping potential diverges toward infinity as we approach the interface. To calculate the probability of the particle sticking to the interface due to the CP forces, we consider the stable and unstable trapping regimes in a cylinder extruded from the exclusion hole. Given that the potential at the edges of our exclusion domain is around $U \simeq -7.5\ k_BT$, the CP potential will start to dominate the gradient force potential around $d \simeq 20$ nm from the interface. By assuming a simple positional averaging for the particle as it travels into the trap and then calculating the volume ratio between the volume where the particle feels an attractive force to the interface and the total volume, the probability of sticking to the surface is given by

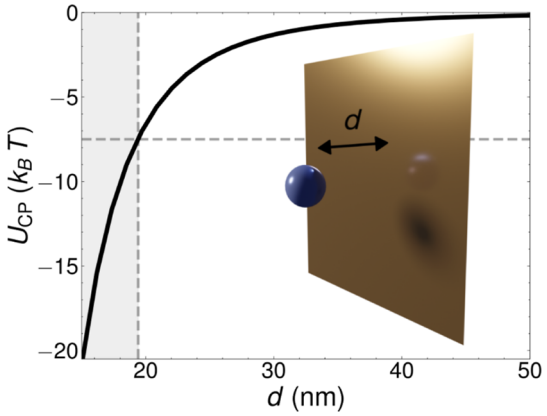


Figure 4. CP trapping potential (U_{CP}) as a function of the distance (d) between the center of a dielectric particle, with a refractive index n = 2 and a radius of R = 15 nm, and an infinite silicon plane with a refractive index n = 3.48. Delimited by the dashed lines is the region (in gray) where the CP potential starts to dominate the gradient force potential. Note that since the distance (d) is measured from the center of the particle, we have excluded from the plot the region where $d < R$ = 15 nm.

$$P_{stick}^{CP}[\%] = \frac{V_{CP}}{V_{total}} = \frac{(R_{exc}^2 - R_{CP}^2)}{R_{exc}^2} \simeq 11.75\% \tag{4}$$

where V_{CP} is the volume fraction where the particle would stick to the interface due to the CP forces, V_{total} is the total volume of the cylindrical exclusion, and R_{CP} denotes the radius where the optical gradient forces dominate the CP forces. As shown in section S3.1 in the Supporting Information, compared to the lightning-rod effect, CP forces will more significantly affect the correct loading of the trap, as it will result in the particle sticking to the dielectric interface with a higher probability, given that $P_{stick}^{CP} \geq P_{stick}^{LR}$, where "LR" denotes the lightning rod. It is important to note that the CP force is inherent to all air-mode cavities, and thus, it is not possible to avoid this source of particles sticking to the surface but only to minimize it by reducing the surface-to-volume ratio near the trapping region. For instance, if one reduced the exclusion region radius, then the surface-to-volume ratio would increase, resulting in even more sticking events due to the CP forces. For example, from the results in Figure 4, an exclusion region radius of 20 nm yields a sticking probability of $P_{stick}^{CP} \simeq 90\%$, which will approach unity as the exclusion becomes even smaller. Therefore, for deeply subwavelength design features, such as the ones in other dielectric nanocavities,[18,19] the CP forces would entirely dominate the optical trapping, making levitated omnidirectional optical trapping unattainable. In other words, vacuum forces set a minimum length scale on the exclusion region radius for levitated omnidirectional trapping in nanostructures, which for this device is around $R_{exc} \simeq 20$ nm. For omnidirectionally trapping nanostructures, the minimum length scale set by CP forces can be reduced by increasing the input power so that optical forces dominate vacuum forces. Therefore, this largely favors dielectric designs compared to plasmonics, since in the considered wavelength range, metals have a much larger imaginary component of the relative permittivity, leading to significantly higher optical losses.

Benchmarking Trapping Performance: Normalized Trapping Stiffness. In the optical trapping community, different metrics are used to benchmark optical trapping platforms of lossless particles; among others, power-normalized trapping

https://doi.org/10.1021/acsphotonics.4c01060
ACS Photonics 2024, 11, 5118−5127

Table 1. Comparison of Different Trapping Platforms in Terms of the Number of Stable Trapping Directions (D), Normalized Trapping Stiffness (η_i), Trapping Stiffness (κ), Sphere Radius (R), Frequency-Dependent Refractive Index of the Particle (n_p), Frequency-Dependent Background Refractive Index (n_{back}), Input Power (P_{in}), and Type of Platform (Plasmonics, Dielectrics, or Optical Tweezers)[a]

Reference	D	η_i [pN/(μm^4·μW)]	κ[fN/nm]	R [nm]	n_p (ω)	n_{back} (ω)	P_{in} [mW]	Platform
50	1	$1.95\cdot10^4$ - $3.62\cdot10^5$	6000 - 7000	25 - 50	1.58	1.33	0.7 - 1.9	Plasmonic (SIBA)
57	1	16.79 - 43.39	3300 - 8530	50	1.59	1.33	1000	Dielectric
58	1	13.18	300	250	1.57	1.33	1	Dielectric (SIBA)
56	2	31.64	4.18	10	0.19 + 5.93i	1.33	9*	Plasmonic (SIBA)
8	2	3.33	2.4	30	0.26 + 6.97i	1.33	1.9	Plasmonic (SIBA)
59	2	-	-	14.5	1.6	1.33	105*	Plasmonic
12	2	-	-	10 - 18	2	1.33	100	Dielectric
60	2	-	-	15 - 60	1.59	1	0.02	Dielectric
20	2	10.71 - 21.41	0.04 - 0.08	10	1.57	1.33	2.5*	Dielectric
15	2	0.06	1.19	50 - 75	1.58	1.33	105*	Dielectric
61	2	-	-	250	1.57	1.33	100	Dielectric
16	3	-	-	50	1.44	1	1	Dielectric (SIBA)
4	3	0.001 - 0.02	0.14 - 2.24**	70	1.44	1	100	Optical tweezer
This work								
λ = 1.55 μm	**3**	**0.36 - 0.42**	**0.46 - 0.53**	**15**	**2**	**1**	**60**	**Dielectric**
λ = 775 nm	**3**	**5.96 - 9.95**	**4.49 - 7.49**	**15**	**2**	**1.33**	**60**	**Dielectric**

[a]To emphasize the number of stable directions, the rows have been colored accordingly, orange for 1 stable direction, yellow for 2 stable directions, and green for omnidirectional trapping with 3 stable directions. We also color the platform text to highlight which platforms lose energy to heating (in red) and which are nearly lossless (in blue). The empty values denoted by "−" were not reported in the references, while we calculated the values marked with * using the light intensity and laser spot size. The value marked with ** was calculated using the fundamental mechanical frequencies of the particle's oscillation in the optical tweezer[4] and its mass, which was calculated from the volume of the particle and the density of fused silica (ρ = 2.2 g/cm^3).

depth,[12,16,55,60] trapping force,[11,12,55,60] and trapping stiffness[4,8,15,50,56] are commonly used. These measures may depend on the physical properties of the trapped particle and its environment, the device footprint, or the input power, making comparisons difficult. Therefore, we propose a normalized trapping stiffness metric (η_i) for optical trapping that normalizes trapping stiffness to particle volume, particle-background permittivity contrast, and input power

$$\eta_i = \frac{\kappa_i \varepsilon_0}{\alpha_R P_{in}} \tag{5}$$

where $i \in \{x, y, z\}$ is an axis index. This metric, which characterizes the power efficiency of optical forces per distance, enables one-to-one comparisons of optical trapping among different platforms. For our trap, we find η_x = 0.42 pN/(μm^4·μW), η_y = 0.36 pN/(μm^4·μW), and η_z = 0.40 pN/(μm^4·μW) along the three axial directions. Note that this metric is not applicable for trapping platforms with no light source, such as vacuum force trapping structures, since there is no input power (P_{in}) and the normalized trapping stiffness η_i diverges. The metric could be modified for these devices by redefining eq 5 without including the input power.

To see how its trapping characteristics compare to other state-of-the-art trapping devices, we have gathered and compared the main trap parameters across several platforms in Table 1, including optical tweezers and plasmonic and dielectric platforms, which may or may not rely on SIBA effects. Note that the devices relying on SIBA effects are only expected to work for sufficiently large (and fixed) particles, unlike optical tweezers and this work, which can be used for all particle sizes as long as the dipole approximation is valid, enabling the trapping of deeply subwavelength particles. The designs presented in this work are the first that provide omnidirectional stable trapping (a trapping potential minimum below $-10\ k_BT$) of particles in nanocavities without relying on the SIBA effect. This has been verified by checking in how many spatial directions the trapping site was in, which was a local minimum of the trapping potential. The number of stable directions has then been added in Table 1 and highlighted with the row coloring. Additionally, and similar to other dielectric devices,[16,57,58] we propose an integrated photonic device, meaning that it is waveguide-coupled, in contrast to many other devices that are excited out of plane by the use of lasers.[8,15,20,50,55,56,59] For these devices, where the laser excitation intensity is reported, we use the laser spot area to compute the total power shown in Table 1. Using the normalized trapping stiffness as an indicator, we observe that devices relying upon plasmonic resonances can achieve stronger normalized trapping stiffnesses[8,50,56,59] than our inverse-designed device. However, plasmonic devices lack omnidirectional trapping, which leads to particles sticking to the surface, and suffer from heating problems due to the optical losses in metals, which can be detrimental in many trapping settings.[11−14,26] We have highlighted this problem in Table 1 by coloring the platforms that lose energy to heating in red and the ones that do not in blue. Regarding dielectric platforms,[15,20,57,58] we see that our platform offers normalized trapping stiffnesses in the same order of magnitude, while being the only non-SIBA solution offering optical trapping in all spatial directions. As previously discussed, for optical trapping nanostructures that do not utilize SIBA effects, there seems to be a trade-off between achieving stability in the spatial directions on the one hand and the normalized trapping stiffness achievable by the optical platforms on the other hand. Compared to optical tweezers, which provide omnidirectional trapping, we achieve similar trapping stiffnesses at significantly lower input power, thus, yielding higher normalized trapping stiffnesses. This demonstrates the usefulness of miniaturizing the free-space optics by means of a waveguide-coupled nanostructured device relying on near-field optical effects. This is also exemplified by comparing the normalized trapping stiffness η_i in Table 1 for our vacuum device (λ = 1.55 μm) and aqueous device (λ = 775 nm), which

https://doi.org/10.1021/acsphotonics.4c01060
ACS Photonics 2024, 11, 5118−5127

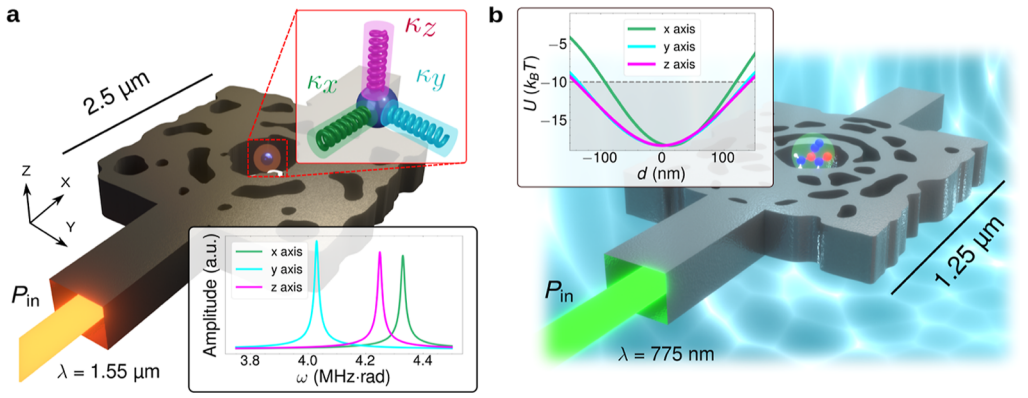


Figure 5. Rendering of the lower half of the inverse-designed structures for two excitation wavelengths. (a) Levitated cavity optomechanical setup, with the frequency response of the mechanical modes of the trapped particle in the three spatial axes. We assume a spectral broadening of 1.5 kHz. (b) Integrated biophotonic setup in an aqueous environment, where a molecule (modeled as a particle with $n = 2$ and $R = 15$ nm) is trapped in a stable omnidirectional potential.

for the same particle size and input power reveal more than an order of magnitude increase of η_i by operating at smaller scales.

Inverse-Designed Nanocavities for Omnidirectional Trapping Applications. The miniaturized integrated circuit shown in Figure 1a bridges the omnidirectional trapping of optical tweezers with the near-field optics of ultracompact nanostructures, thereby enabling a range of chip-scale applications. As an example, we demonstrate its potential in levitated cavity optomechanics. Owing to the harmonic potential close to the cavity center, we calculate the natural frequencies of the harmonic oscillator for the different axes as $\Omega_{0,i} = \sqrt{\kappa_i/m}$, where m is the mass of the particle and $i \in \{x, y, z\}$ is an axis index. Using a density of $\rho = 2$ g/cm^3, which represents particles like proteins ($\rho \in [1.4\text{–}1.5$ g/cm$^3]$)[62] and quantum dots (e.g., $\rho_{Si} = 2.33$ g/cm^3, $\rho_{GaAs} = 5.32$ g/cm^3), we find $\Omega_{0,x} = 4.33$ rad·MHz, $\Omega_{0,y} = 4.03$ rad·MHz, and $\Omega_{0,z} = 4.25$ rad·MHz. In the quantum-mechanical limit, the mean thermal occupancy of the mechanical energy states is given by $\langle n \rangle = k_B T/\hbar\Omega_0$,[4] where $\hbar$ is the reduced Planck constant. Resolving the quantum ground state requires $\langle n \rangle < 1$, which with the natural frequencies of this system requires center-of-mass equilibrium temperatures of $T_x = 0.21$ mK, $T_y = 0.19$ mK, and $T_z = 0.20$ mK. These temperatures are 2 orders of magnitude higher than for conventional optical tweezers,[4] which combined with the particle-size agnostic omnidirectional trapping facilitates mesoscopic quantum optomechanical experiments with optically trapped and cooled nanoparticles. One could potentially reach these temperatures by lowering the ambient temperature while employing methods like parametric feedback cooling in a vacuum chamber.[4] A representation of the optomechanical system is shown in Figure 5a.

To demonstrate the versatility of the design framework, we move toward near-infrared frequencies and design a device suited for integrated biological sensing. For biological characterization in aqueous environments, it is crucial to operate within the biological window,[63] a spectral range where light has a long penetration depth in tissue and water has low optical losses. This helps alleviate losing too much energy to heating, which could otherwise compromise the trapping setup.[11−14] Although the optical losses of water may be lower for wavelengths below the biological window, optical losses in silicon become larger, which would lead to a reduction in the efficiency of our device. To this end, we scale all geometric design parameters and the wavelength by half, shifting toward the near-infrared frequencies at $\lambda = 775$ nm. Accordingly, we set the background refractive index to water and adjusted the refractive index of silicon. With these new design parameters, we resolve the optimization problem and obtain the trap design in Figure 5b. This trap yields an omnidirectional stable trap for a single particle at the center of the design, with trapping stiffnesses of $\kappa_x = 7.49$ fN/nm, $\kappa_y = 4.49$ fN/nm, and $\kappa_z = 4.77$ fN/nm, for a particle with radius $R = 15$ nm and for an input power of $P_{in} = 60$ mW. The normalized trapping stiffnesses for this device are $\eta_x = 9.95$ pN/(μm^4·μW), $\eta_y = 5.96$ pN/(μm^4·μW), and $\eta_z = 6.33$ pN/(μm^4·μW). These values are larger than those of the device operating in the short-wave infrared due to the smaller footprint of the device: given that both devices are fed with the same input power and trap exactly the same particle, halving all of the geometric design parameters results in an increased trapping stiffness, since the stiffness is given as a force per unit distance. The inversely designed optical trapping device is thus an integrated optical component capable of stably trapping biomolecules in all spatial dimensions in an aqueous solution. Note that omnidirectional trapping still holds for lower values of the refractive index of molecules (e.g., $n \approx 1.5$).[51] One could envision using the platform, represented in Figure 5b, integrated with an optical detection scheme to trap and detect particles in situ in biological environments, opening a path for the development of new experiments and technologies in integrated biophotonics systems.

CONCLUSIONS

The omnidirectional trapping of subwavelength nanoparticles in integrated optical devices is central to many applications in the field of optical trapping, such as microbiology,[2,3] biophysics,[42] or fundamental physics.[4−6] For deeply subwavelength particles, where the dipole approximation is valid, we demonstrate that it is possible to tailor the electric field distribution and the trapping potential by careful nanostructuring of the dielectric environment. The target distribution of the electric fields results in a particle-size-agnostic omnidirectional optical trap based on gradient forces. We test the geometric limits of omnidirectional trapping by means of a parametric study that indicates omnidirectional trapping only for exclusion radii above $R_{exc} \geq 250$ nm and demonstrate how CP forces also set a lower size limit for the exclusion radius (R_{exc}). To compare the optimized device to other nanophotonic platforms, we propose the metric of normalized trapping stiffness (η_i), which shows unprece-

https://doi.org/10.1021/acsphotonics.4c01060
ACS Photonics 2024, 11, 5118−5127

dented values compared to other state-of-the art optical tweezer platforms,[4] highlighting the deeply subwavelength nature of the trapped particles and the low input power required for trapping. Moreover, our framework enables the design of manufacturable[18] optical traps for a given application by rescaling the wavelength and the spatial dimensions of the device and adjusting the material parameters accordingly, before applying the inverse-design process. We have demonstrated this at short-wave-infrared (λ = 1.55 μm) and near-infrared frequencies (λ = 775 nm). Since the designs can be fabricated by standard electron-beam lithography, we anticipate experimental realizations of the optical traps, with applications in levitated cavity optomechanics and integrated biophotonics technologies.

We also foresee developments in our inverse-design framework. For instance, modifications to the FOM and the optimization framework can enable the design of optical traps based on different materials, traps for lossy or resonant particles, traps with multiple trapping spots, or novel optical traps for multiple quantum emitters such as quantum dots or cold atoms. These networks of trapped emitters may, in turn, be used to study and develop quantum many-body systems.[36]

■ ASSOCIATED CONTENT

Supporting Information

The Supporting Information is available free of charge at https://pubs.acs.org/doi/10.1021/acsphotonics.4c01060.

Theoretical description of forces in optical trapping; inverse-design framework, detailing the formulation of the forward and the optimization problem; and effect of optical surface forces when loading the particle in the inverse-designed nanostructures (PDF)

■ AUTHOR INFORMATION

Corresponding Authors

Beñat Martinez de Aguirre Jokisch − *Department of Civil and Mechanical Engineering, Technical University of Denmark, Kongens Lyngby 2800, Denmark; NanoPhoton—Center for Nanophotonics, Technical University of Denmark, Kongens Lyngby 2800, Denmark;* orcid.org/0009-0009-2725-6288; Email: bmdaj@dtu.dk

Benjamin Falkenberg Gøtzsche − *Department of Electrical and Photonics Engineering, Technical University of Denmark, Kongens Lyngby 2800, Denmark; NanoPhoton—Center for Nanophotonics, Technical University of Denmark, Kongens Lyngby 2800, Denmark*; Email: bfago@dtu.dk

Philip Trøst Kristensen − *Department of Electrical and Photonics Engineering, Technical University of Denmark, Kongens Lyngby 2800, Denmark; NanoPhoton—Center for Nanophotonics, Technical University of Denmark, Kongens Lyngby 2800, Denmark*; Email: ptkr@dtu.dk

Martijn Wubs − *Department of Electrical and Photonics Engineering, Technical University of Denmark, Kongens Lyngby 2800, Denmark; NanoPhoton—Center for Nanophotonics, Technical University of Denmark, Kongens Lyngby 2800, Denmark*; Email: mwubs@dtu.dk

Ole Sigmund − *Department of Civil and Mechanical Engineering, Technical University of Denmark, Kongens Lyngby 2800, Denmark; NanoPhoton—Center for Nanophotonics, Technical University of Denmark, Kongens Lyngby 2800, Denmark*; Email: olsi@dtu.dk

Rasmus Ellebæk Christiansen − *Department of Civil and Mechanical Engineering, Technical University of Denmark, Kongens Lyngby 2800, Denmark; NanoPhoton—Center for Nanophotonics, Technical University of Denmark, Kongens Lyngby 2800, Denmark*; Email: raelch@dtu.dk

Complete contact information is available at: https://pubs.acs.org/10.1021/acsphotonics.4c01060

Notes

The authors declare no competing financial interest.

■ ACKNOWLEDGMENTS

We would like to thank Jesper Mørk for the useful discussions and support. B.F.G., P.T.K., and M.W. would also like to thank Kishan Dholakia for the useful discussions. We gratefully acknowledge financial support from the Danish National Research Foundation through NanoPhoton—Center for Nanophotonics, grant number DNRF147.

■ REFERENCES

(1) Ashkin, A. Acceleration and Trapping of Particles by Radiation Pressure. *Phys. Rev. Lett.* **1970**, *24*, 156−159.

(2) Sudhakar, S.; Abdosamadi, M. K.; Jachowski, T. J.; Bugiel, M.; Jannasch, A.; Schäffer, E. Germanium nanospheres for ultraresolution picotensiometry of kinesin motors. *Science* **2021**, *371*, No. eabd9944.

(3) Ashkin, A.; Dziedzic, J. M.; Yamane, T. Optical trapping and manipulation of single cells using infrared laser beams. *Nature* **1987**, *330*, 769−771.

(4) Gieseler, J.; Deutsch, B.; Quidant, R.; Novotny, L. Subkelvin Parametric Feedback Cooling of a Laser-Trapped Nanoparticle. *Phys. Rev. Lett.* **2012**, *109*, 103603.

(5) Dholakia, K.; Zemánek, P. Colloquium: Gripped by light: Optical binding. *Rev. Mod. Phys.* **2010**, *82*, 1767−1791.

(6) Donato, M. G.; Mazzulla, A.; Pagliusi, P.; Magazzù, A.; Hernandez, R. J.; Provenzano, C.; Gucciardi, P. G.; Maragò, O. M.; Cipparrone, G. Light-induced rotations of chiral birefringent microparticles in optical tweezers. *Sci. Rep.* **2016**, *6*, 31977.

(7) Maragò, O. M.; Jones, P. H.; Gucciardi, P. G.; Volpe, G.; Ferrari, A. C. Optical trapping and manipulation of nanostructures. *Nat. Nanotechnol.* **2013**, *8*, 807−819.

(8) Mestres, P.; Berthelot, J.; Aćimović, S. S.; Quidant, R. Unraveling the optomechanical nature of plasmonic trapping. *Light: Sci. Appl.* **2016**, *5*, No. e16092.

(9) Jones, S.; Al Balushi, A. A.; Gordon, R. Raman spectroscopy of single nanoparticles in a double-nanohole optical tweezer system. *J. Opt.* **2015**, *17*, 102001.

(10) Pang, Y.; Gordon, R. Optical Trapping of a Single Protein. *Nano Lett.* **2012**, *12*, 402−406.

(11) Xu, Z.; Crozier, K. B. All-dielectric nanotweezers for trapping and observation of a single quantum dot. *Opt. Express* **2019**, *27*, 4034−4045.

(12) Hernández-Sarria, J.; Oliveira, O. N.; Mejía-Salazar, J. Toward Lossless Infrared Optical Trapping of Small Nanoparticles Using Nonradiative Anapole Modes. *Phys. Rev. Lett.* **2021**, *127*, 186803.

(13) Mejía-Salazar, J. R.; Oliveira, O. N. J. Plasmonic Biosensing. *Chem. Rev.* **2018**, *118*, 10617−10625.

(14) Wang, K.; Crozier, K. B. Plasmonic trapping with a gold nanopillar. *ChemPhysChem* **2012**, *13*, 2639−2648.

(15) Conteduca, D.; Khan, S. N.; Martínez Ruiz, M. A.; Bruce, G. D.; Krauss, T. F.; Dholakia, K. Fano Resonance-Assisted All-Dielectric Array for Enhanced Near-Field Optical Trapping of Nanoparticles. *ACS Photonics* **2023**, *10*, 4322−4328.

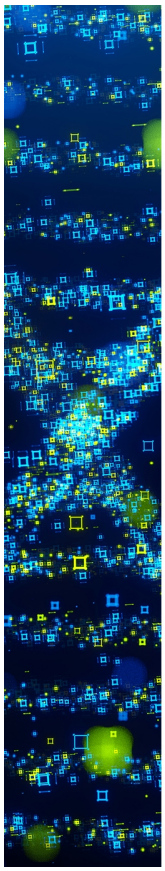
(16) Maňka, T.; Šiler, M.; Liška, V.; Zemánek, P.; Šerý, M.; Brzobohatý, O. Simulation of optomechanical interaction of levitated nanoparticle with photonic crystal micro cavity. *Opt. Express* **2024**, *32*, 7185−7196.

(17) Hu, S.; Khater, M.; Salas-Montiel, R.; Kratschmer, E.; Engelmann, S.; Green, W. M. J.; Weiss, S. M. Experimental realization

of deep-subwavelength confinement in dielectric optical resonators. *Sci. Adv.* **2018**, *4*, No. eaat2355.
(18) Albrechtsen, M.; Vosoughi Lahijani, B.; Christiansen, R. E.; Nguyen, V. T. H.; Casses, L. N.; Hansen, S. E.; Stenger, N.; Sigmund, O.; Jansen, H.; Mørk, J.; Stobbe, S. Nanometer-scale photon confinement in topology-optimized dielectric cavities. *Nat. Commun.* **2022**, *13*, 6281.
(19) Babar, A. N.; Weis, T. A. S.; Tsoukalas, K.; Kadkhodazadeh, S.; Arregui, G.; Vosoughi Lahijani, B.; Stobbe, S. Self-assembled photonic cavities with atomic-scale confinement. *Nature* **2023**, *624*, 57−63.
(20) Xu, Z.; Song, W.; Crozier, K. B. Optical Trapping of Nanoparticles Using All-Silicon Nanoantennas. *ACS Photonics* **2018**, *5*, 4993−5001.
(21) Yoon, S. J.; Lee, J.; Han, S.; Kim, C.-K.; Ahn, C. W.; Kim, M.-K.; Lee, Y.-H. Non-fluorescent nanoscopic monitoring of a single trapped nanoparticle via nonlinear point sources. *Nat. Commun.* **2018**, *9*, 2218.
(22) Brunetti, G.; Sasanelli, N.; Armenise, M. N.; Ciminelli, C. Nanoscale Optical Trapping by Means of Dielectric Bowtie. *Photonics* **2022**, *9*, 425.
(23) Hu, S.; Weiss, S. M. Design of Photonic Crystal Cavities for Extreme Light Concentration. *ACS Photonics* **2016**, *3*, 1647−1653.
(24) Choi, H.; Heuck, M.; Englund, D. Self-Similar Nanocavity Design with Ultrasmall Mode Volume for Single-Photon Nonlinearities. *Phys. Rev. Lett.* **2017**, *118*, 223605.
(25) Albrechtsen, M.; Vosoughi Lahijani, B.; Stobbe, S. Two regimes of confinement in photonic nanocavities: bulk confinement versus lightning rods. *Opt. Express* **2022**, *30*, 15458−15469.
(26) Ishida, T.; Murayama, T.; Taketoshi, A.; Haruta, M. Importance of Size and Contact Structure of Gold Nanoparticles for the Genesis of Unique Catalytic Processes. *Chem. Rev.* **2020**, *120*, 464−525.
(27) Neumeier, L.; Quidant, R.; Chang, D. E. Self-induced back-action optical trapping in nanophotonic systems. *New J. Phys.* **2015**, *17*, 123008.
(28) Jensen, J. S.; Sigmund, O. Systematic design of photonic crystal structures using topology optimization: Low-loss waveguide bends. *Appl. Phys. Lett.* **2004**, *84*, 2022−2024.
(29) Wang, F.; Jensen, J. S.; Sigmund, O. Robust topology optimization of photonic crystal waveguides with tailored dispersion properties. *J. Opt. Soc. Am. B* **2011**, *28*, 387−397.
(30) Wang, F.; Christiansen, R. E.; Yu, Y.; Mørk, J.; Sigmund, O. Maximizing the quality factor to mode volume ratio for ultra-small photonic crystal cavities. *Appl. Phys. Lett.* **2018**, *113*, 241101.
(31) Liang, X.; Johnson, S. G. Formulation for scalable optimization of microcavities via the frequency-averaged local density of states. *Opt. Express* **2013**, *21*, 30812−30841.
(32) Piggott, A. Y.; Lu, J.; Lagoudakis, K. G.; Petykiewicz, J.; Babinec, T. M.; Vučković, J. Inverse design and demonstration of a compact and broadband on-chip wavelength demultiplexer. *Nat. Photonics* **2015**, *9*, 374−377.
(33) Ahn, G. H.; Yang, K. Y.; Trivedi, R.; White, A. D.; Su, L.; Skarda, J.; Vučković, J. Photonic Inverse Design of On-Chip Microresonators. *ACS Photonics* **2022**, *9*, 1875−1881.
(34) Zhou, M.; Lazarov, B. S.; Wang, F.; Sigmund, O. Minimum length scale in topology optimization by geometric constraints. *Comput. Methods Appl. Mech. Eng.* **2015**, *293*, 266−282.
(35) Li, Q.; Chen, W.; Liu, S.; Tong, L. Structural topology optimization considering connectivity constraint. *Struct. Multidiscip. Optim.* **2016**, *54*, 971−984.
(36) Chang, D.; Douglas, J.; González-Tudela, A.; Hung, C.-L.; Kimble, H. Colloquium: Quantum matter built from nanoscopic lattices of atoms and photons. *Rev. Mod. Phys.* **2018**, *90*, 031002.
(37) Novotny, L.; Hecht, B. *Principles of Nano-Optics*, 2nd ed.; Cambridge University Press: Cambridge, 2012.
(38) Erickson, H. P. Size and Shape of Protein Molecules at the Nanometer Level Determined by Sedimentation, Gel Filtration, and Electron Microscopy. *Biol. Proced. Online* **2009**, *11*, 32−51.
(39) Wang, L.-W.; Zunger, A. Pseudopotential calculations of nanoscale CdSe quantum dots. *Phys. Rev. B: Condens. Matter Mater. Phys.* **1996**, *53*, 9579−9582.
(40) Holewa, P.; Kadkhodazadeh, S.; Gawełczyk, M.; Baluta, P.; Musiał, A.; Dubrovskii, V. G.; Syperek, M.; Semenova, E. Droplet epitaxy symmetric InAs/InP quantum dots for quantum emission in the third telecom window: morphology, optical and electronic properties. *Nanophotonics* **2022**, *11*, 1515−1526.
(41) Protesescu, L.; Yakunin, S.; Bodnarchuk, M. I.; Krieg, F.; Caputo, R.; Hendon, C. H.; Yang, R. X.; Walsh, A.; Kovalenko, M. V. Nanocrystals of Cesium Lead Halide Perovskites (CsPbX3, X = Cl, Br, and I): Novel Optoelectronic Materials Showing Bright Emission with Wide Color Gamut. *Nano Lett.* **2015**, *15*, 3692−3696.
(42) Bustamante, C. J.; Chemla, Y. R.; Liu, S.; Wang, M. D. Optical tweezers in single-molecule biophysics. *Nat. Rev. Methods Primers* **2021**, *1*, 25−29.
(43) Jin, J.-M. *The Finite Element Method in Electromagnetics*, 3rd ed.; IEEE Press: Piscataway, NJ, 2014.
(44) Wang, F.; Lazarov, B. S.; Sigmund, O. On projection methods, convergence and robust formulations in topology optimization. *Struct. Multidiscip. Optim.* **2011**, *43*, 767−784.
(45) Christiansen, R. E.; Sigmund, O. Compact 200 line MATLAB code for inverse design in photonics by topology optimization: tutorial. *J. Opt. Soc. Am. B* **2021**, *38*, 510−520.
(46) Christiansen, R. E.; Vester-Petersen, J.; Madsen, S. P.; Sigmund, O. A non-linear material interpolation for design of metallic nanoparticles using topology optimization. *Comput. Methods Appl. Mech. Eng.* **2019**, *343*, 23−39.
(47) Svanberg, K. The method of moving asymptotes—a new method for structural optimization. *Int. J. Numer. Methods Eng.* **1987**, *24*, 359−373.
(48) *COMSOL MultiphysicsV. 6.1*; COMSOL AB: Stockholm, Sweden, 2022, www.comsol.com (accessed June 10, 2024).
(49) DTU Computing Center. DTU Computing Center Resources, 2024.
(50) Juan, M. L.; Gordon, R.; Pang, Y.; Eftekhari, F.; Quidant, R. Self-induced back-action optical trapping of dielectric nanoparticles. *Nat. Phys.* **2009**, *5*, 915−919.
(51) Jokisch, B. M. d. A.; Sigmund, O.; Christiansen, R. E. Inverse design of dielectric nanostructures for optical trapping. *Nanosci., NanoEng. Appl.* **2024**, in press.
(52) Casimir, H. B. G.; Polder, D. The Influence of Retardation on the London-van der Waals Forces. *Phys. Rev.* **1948**, *73*, 360−372.
(53) Intravaia, F.; Henkel, C.; Antezza, M. *Fluctuation-induced Forces between Atoms and Surfaces: The Casimir-Polder Interaction*; Springer: Berlin Heidelberg, 2011; pp 345−391.
(54) Paulus, M.; Gay-Balmaz, P.; Martin, O. J. F. Accurate and efficient computation of the Green's tensor for stratified media. *Phys. Rev. E: Stat. Phys., Plasmas, Fluids, Relat. Interdiscip. Top.* **2000**, *62*, 5797−5807.
(55) Hernández-Sarria, J. J.; Oliveira, O. N. J.; Mejía-Salazar, J. R. Numerical Simulations of Double-Well Optical Potentials in All-Dielectric Nanostructures for Manipulation of Small Nanoparticles in Aqueous Media. *ACS Appl. Nano Mater.* **2023**, *6*, 1405−1412.
(56) Bouloumis, T. D.; Kotsifaki, D. G.; Nic Chormaic, S. Enabling Self-Induced Back-Action Trapping of Gold Nanoparticles in Metamaterial Plasmonic Tweezers. *Nano Lett.* **2023**, *23*, 4723−4731.
(57) Mandal, S.; Serey, X.; Erickson, D. Nanomanipulation Using Silicon Photonic Crystal Resonators. *Nano Lett.* **2010**, *10*, 99−104.
(58) Tonin, M.; Mor, F. M.; Forró, L.; Jeney, S.; Houdré, R. Thermal fluctuation analysis of singly optically trapped spheres in hollow photonic crystal cavities. *Appl. Phys. Lett.* **2016**, *109*, 241107.
(59) Nelson, D.; Kim, S.; Crozier, K. B. Inverse Design of Plasmonic Nanotweezers by Topology Optimization. *ACS Photonics* **2024**, *11*, 85−92.
(60) Wang, J.; Wang, C.; Han, Z.; Tian, H. On-chip trapping and sorting of nanoparticles using a single slotted photonic crystal nanobeam cavity. *Opt. Express* **2022**, *30*, 11192.
(61) Tonin, M.; Descharmes, N.; Houdré, R. Hybrid PDMS/glass microfluidics for high resolution imaging and application to sub-wavelength particle trapping. *Lab Chip* **2016**, *16*, 465−470.

https://doi.org/10.1021/acsphotonics.4c01060
ACS Photonics 2024, 11, 5118−5127

(62) Fischer, H.; Polikarpov, I.; Craievich, A. F. Average protein density is a molecular-weight-dependent function. *Protein Sci.: Publ. Protein Soc.* **2004**, *13*, 2825−2828.
(63) Feng, Z.; Tang, T.; Wu, T.; Yu, X.; Zhang, Y.; Wang, M.; Zheng, J.; Ying, Y.; Chen, S.; Zhou, J.; Fan, X.; Zhang, D.; Li, S.; Zhang, M.; Qian, J. Perfecting and extending the near-infrared imaging window. *Light: Sci. Appl.* **2021**, *10*, 197.


CAS BIOFINDER DISCOVERY PLATFORM™
STOP DIGGING THROUGH DATA —START MAKING DISCOVERIES
CAS BioFinder helps you find the right biological insights in seconds
Start your search
CAS
A division of the American Chemical Society

https://doi.org/10.1021/acsphotonics.4c01060
ACS Photonics 2024, 11, 5118−5127